71st International Astronautical Congress (IAC) – The CyberSpace Edition, 12-14 October 2020.


IAC-20.C1.5.13.x58119

# Target Selection for M-ARGO Interplanetary CubeSat

**Vittorio Franzese[1], Carmine Giordano[2], Yang Wang[3], Francesco Topputo[4], Hannah Goldberg[5], Alfonso Gonzalez[6], Roger Walker[7]**

The Miniaturised Asteroid Remote Geophysical Observer (M-ARGO) is planned to be the first standalone CubeSat mission to rendezvous with and characterise a near-Earth asteroid for the presence of in-situ resources. Beside carrying out the scientific tasks, M-ARGO is a tremendous demonstrator of miniaturised deep-space technologies currently under development in the ESA Technology Programme. The M-ARGO mission concept was originally conceived by ESA's Concurrent Design Facility (CDF) team in 2017. The Phase A project was led by GomSpace Luxembourg and supported by Politecnico di Milano in 2019–2020, under ESA GSTP contract. This work presents the initial results for what concerns the mission analysis and design of M-ARGO. In particular, we show the original procedure developed to assess the reachable NEO targets and the subsequent down-selection process. An in-house indirect solver, the Low-Thrust Trajectory Optimiser (LT2.0), has been used in combination with a realistic thruster model, featuring variable input power, thrust, and specific impulse. The solver implements an accurate switching detection technique along with analytic derivatives. Hundreds of both time- and fuel-optimal problems have been solved, aiming at near-Earth asteroids properly filtered from the Minor Planet Center Database. The analyses show that approximately 150 minor bodies are found potentially reachable by M-ARGO when departing from Sun-Earth L2 within a 3-year transfer duration. Out of these, 41 targets have been down-selected, and a short list of the 5 most promising objects has been extracted. Our preliminary results indicate mission feasibility. Overall, M-ARGO has the potential to enable a completely new class of low-cost, deep space exploration missions.

## 1 Introduction

ESA has funded several interplanetary CubeSat mission studies like M-ARGO (Miniaturized Asteroid Remote Geophysical Observer) [1, 2], LUMIO (Lunar Meteoroid Impacts Observer) [3, 4, 5, 6], and CubeSats along the Hera mission [7]; NASA has funded several SmallSat deep-space mission studies after Mars Cube One (MarCO) [8]. M-ARGO is planned to be the first ESA stand-alone CubeSat mission to rendezvous with a near-Earth asteroid (NEA) [1, 9]. The M-ARGO concept was initially developed by ESA's Concurrent Design Facility (CDF) team in 2017 [10]. Phase A study was performed in 2019-2020 with GomSpace Luxembourg and Polimi to assess mission feasibility including NEO target selection, mission analysis, spacecraft design, and programmatic plan. The M-ARGO mission objectives are to: (1) Demonstrate the capability of CubeSat nanospacecraft systems to independently explore deep space for the first time; (2) Rendezvous with a Near Earth Object (NEO) and characterize its physical properties for the presence of in-situ resources; (3) Advance miniaturized technologies currently under development in Europe; (4) Test autonomous GNC techniques and components performance during transfer to target object.

This work deals with the NEO targets screening for the M-ARGO mission. The list of asteroids has been retrieved by the Minor Planet Center[1] and filtered considering time-optimal and fuel-optimal transfers from the Sun-Earth L2 point to the asteroids location. Then, a short-list of 5 candidate targets is produced by a working group made by ESA, GomSpace, Politecnico di Milano and the Small Body community. These targets are later considered for a dedicated mission analysis.

The paper is structured as follows. Section 2 reports the approach for the NEO targets screening. Section 3 details the first database filtering step. Section 4 summarizes the assumptions made for the platform and the mission. Then, the methodology and the results for the time-optimal transfers and fuel-optimal transfers are

[1]PhD Candidate, Department of Aerospace Science and Technology, Politecnico di Milano, Via La Masa 34, 20156, Milano, Italy, vittorio.franzese@polimi.it
[2]PhD Candidate, Department of Aerospace Science and Technology, Politecnico di Milano, Via La Masa 34, 20156, Milano, Italy, carmine.giordano@polimi.it
[3]PhD Candidate, Department of Aerospace Science and Technology, Politecnico di Milano, Via La Masa 34, 20156, Milano, Italy, yang.wang@polimi.it
[4]Associate Professor, Department of Aerospace Science and Technology, Politecnico di Milano, Via La Masa 34, 20156, Milano, Italy, francesco.topputo@polimi.it
[5]Systems Engineer, GomSpace Aps, Langagervej 6, 9220 Aalborg, Denmark, hrg@gomspace.com
[6]Systems Engineer, GomSpace Aps, United States, alfonso8gonzalez@gmail.com
[7]Head of CubeSat Systems Unit, European Space Research & Technology Centre (ESTEC), ESA, Postbus 299, 2200 AG, Noordwijk, The Netherlands, roger.walker@esa.int

[1]See `https://minorplanetcenter.net/`

shown in Section 5 and Section 6, respectively. The reachable targets and their statistics are summarized in Section 7 and Section 8. Then, this list is further reduced with the criteria in Section 9. The final shortlist of targets is presented in Sections 10 and 11. Conclusions are drawn in Section 12.

## 2 Approach

The objective of the M-ARGO mission is to rendezvous with a near-Earth asteroid to characterize its physical properties and assess the potential for future resource exploitation. Thus, it is required to identify the subset of asteroids that are reachable considering the constraints of a 12U deep-space CubeSat. Figure 1 shows the approach followed to filter the database of known asteroids to produce the reachable asteroids shortlist. Note that the final shortlist and the final target selection are made by a working group involving ESA, the small-body community, and the M-ARGO consortium (GomSpace Luxembourg and Politecnico di Milano). The procedure is the following:

1-2 **Database retrieval.** The Minor Planet Center (MPC) Database[1] is considered as the source of information for the minor planets in the Solar System. It comprehends the designation and the orbit computation of all the discovered minor planets and it is updated daily. More than 900,000 objects are accounted for as of October 2020.

3-4 **Pre-Filtering.** The full list of asteroids is pre-filtered using ranges of orbital parameters. Educated guesses on these parameters have been inferred from [9]. These involve capping the aphelion, bottoming the perihelion, and bounding the inclination as well as the number of observations. This filtering reduces the full list of asteroids to a preliminary list of approximately 500 potential targets; see Section 3.

5-6 **Time-optimal transfers.** A massive search is conducted to compute time-optimal transfers to each of the asteroids in the preliminary list. The optimisation considers the two-body problem with the realistic thruster model in Section 4.2, departure from Sun–Earth $L_2$, and departure window as specified in Section 4.1. The aim of this step is to determine the *minimum theoretical transfer time* to each asteroid for each departure epoch. The objects whose minimum transfer time is greater than 3 years are filtered-out.

7 **Time-optimal ranking.** The filtered time-optimal solutions are ordered to produce a time-optimal ranking. The number of targets is then reduced to $\sim 170$ objects; see Section 5.

8-9 **Fuel-optimal transfers.** The objects resulting feasible after the time-optimal analysis are processed under the perspective of a fuel-optimal optimisation, using the same model and boundary conditions as in the time-optimal optimisation. This analysis finds the minimum propellant mass for each combination of departure epoch and transfer time. The objects whose minimum required propellant mass is greater than 2.8 kg are excluded from the list.

10 **Fuel-optimal ranking.** The fuel-optimal solutions as output of step 9 are ordered to produce a fuel-optimal ranking made of approximately 150 reachable objects; see Section 6.

11 **Lists of ranked optimal solutions.** The ranked lists of time-optimal and fuel-optimal solutions produced as output of the filtering chain has been examined by GomSpace, Politecnico di Milano, the small body community, and ESA. The list of the 5 shortlisted targets is reported in Section 11.

## 3 Minor planets database filtering

The Minor Planet Center accounts for more than 900,000 objects in the Solar System. Figure 2a shows the semi-major axis ($a$) versus the eccentricity ($e$) for all the observed objects as a scatter plot (black dots), while Figure 2b displays the semi-major axis ($a$) versus the inclination ($i$) for the same bodies (black dots).
The subset of potential targets has been defined by restricting the aphelium ($r_a$) upper bound (UB) to 1.25 AU and the perihelium ($r_p$) lower bound (LB) to 0.75 AU. Moreover, in order to comply with realistic CubeSat propulsive capabilities, an upper bound on the inclination equal to 10 degrees has been set. Finally, a lower bound of 10 observations ($N_{obs}$) is enforced to assure accuracy in the orbital elements of the asteroids. Table 1 summarises the filtering parameters used.

Tab. 1: NEO database filtering parameters.

| **Parameter** | Lower Bound | Upper Bound |
|---|---|---|
| $r_a$ | – | 1.25 AU |
| $r_p$ | 0.75 AU | – |
| $i$ | 0 deg | 10 deg |
| $N_{obs}$ | 10 | – |

[1] See `https://minorplanetcenter.net/`

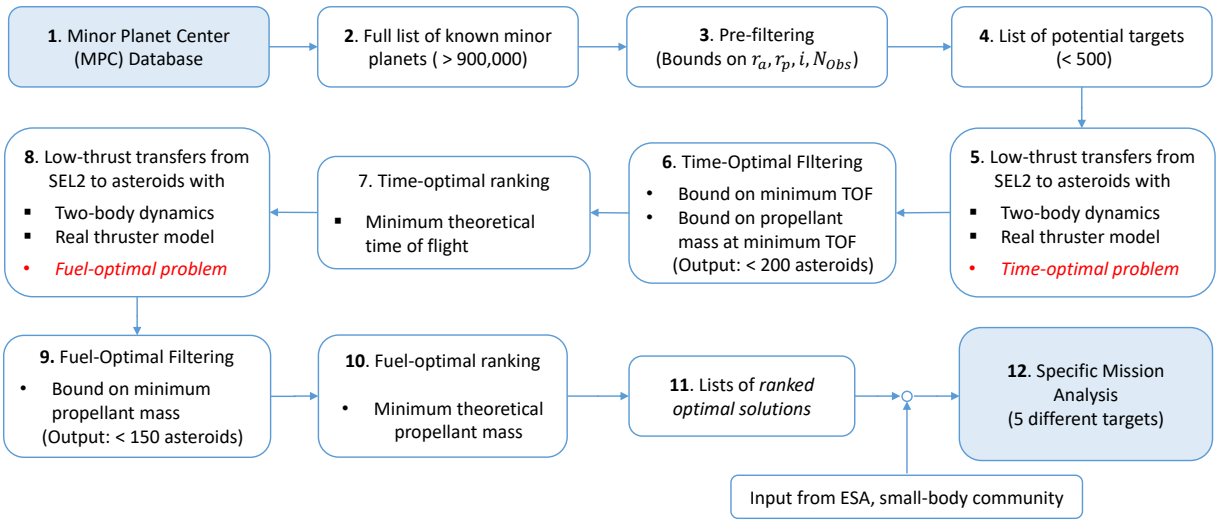


Fig. 1: Methodology of the NEO target screening.

The constraints in terms of $r_a$, $r_p$, and $i$ are shown in Figure 2 as well. The solid and the dashed lines in Figure 2a represent the projection of the perihelium and aphelium bounds on the $(a, e)$ plane, respectively. The solid horizontal line in Figure 2b is the upper bound on the inclination. The asteroids that satisfy the bounds in Table 1 are highlighted orange in Figure 2.

Figure 3 shows the estimated size versus the rotational period of the asteroids catalogued in the Asteroid Lightcurve Database (LCDB[1]). The plot highlights the so called spin barrier (red dashed line). Most of the big asteroids (with a diameter larger than 1 km) lie below the spin barrier, meaning that they have a rotational period higher than 2 hours. The small asteroids have a rotational period that can be in the order of 1 hour or less. The filtered asteroids are highlighted in orange in Figure 3; they lie in the region of the fast rotators.

## 4 Assumptions

This section reports the assumptions made for the mission and the spacecraft as inputs to the time-optimal and fuel-optimal filtering steps.

### *4.1 Mission and spacecraft data*

The departure from the Sun–Earth L2 point (SEL2) is set in the window 1 Jan 2023—31 Dec 2024. The considered transfer duration is up to 3 years, and the close-proximity operations last up to 6 months. The spacecraft mass is 26.4 kg and the propellant mass is 2.8 kg. The Sun-projected area is 0.30 m$^2$ and the reflectivity coefficient is 1.3.

[1]See `http://www.minorplanet.info/lightcurvedatabase.html`

### *4.2 Thruster model*

The mission analysis implements a realistic thruster model, that is, a model mapping maximum thrust and specific impulse variation over the instantaneous input power. The thruster model assumes that both the maximum thrust, $T_{max}$, and the specific impulse, $I_{sp}$, depend on the instantaneous engine input power, $P_{in}$, which in turn is a function of the Sun distance, $r$. These functions have been handled using fourth-order polynomials, which represent surrogate models of the miniaturized ion thruster as well as the power production and distribution units to be used in M-ARGO. Fourth-order polynomials allow capturing the complexities of these systems when used in conjunction, while still assuring smooth, non-singular derivatives:

$$T_{max} = a_0 + a_1 P_{in} + a_2 P_{in}^2 + a_3 P_{in}^3 + a_4 P_{in}^4 \quad (1)$$

$$I_{sp} = b_0 + b_1 P_{in} + b_2 P_{in}^2 + b_3 P_{in}^3 + b_4 P_{in}^4 \quad (2)$$

$$P_{in} = c_0 + c_1 r + c_2 r^2 + c_3 r^3 + c_4 r^4 \quad (3)$$

Beside the variation in Eq. (3), the thruster input power is bounded within a minimum and maximum value, $P_{in,min}$ and $P_{in,max}$, respectively, for technological limits. Although the value of the 15 coefficients $\{a_i, b_i, c_i\}$, $i = 0, \ldots, 4$, in Eqs. (1)–(3) as well as those for $P_{in,min}$ and $P_{in,max}$ will be known with greater confidence in later stages of the design, preliminary design values have been provided by GomSpace, using the specifications in [11]. The coefficients and the input power limits used in the mission analysis are given in Table 2.

Figure 4 shows the performances of the thruster model.

Tab. 2: Thruster model coefficients

| $T_{max}$ | Value | Unit | $I_{sp}$ | Value | Unit | $P_{in}$ | Value | Unit |
|---|---|---|---|---|---|---|---|---|
| $a_0$ | $-1.2343$ | mN | $b_0$ | $-5519.5$ | s | $c_0$ | 840.11 | W |
| $a_1$ | 0.026498 | mN/W | $b_1$ | 225.44 | s/W | $c_1$ | -1754.3 | W/AU |
| $a_2$ | 0 | | $b_2$ | $-1.8554$ | s/$W^2$ | $c_2$ | 1625.01 | W/AU$^2$ |
| $a_3$ | 0 | | $b_3$ | 0.005084 | s/$W^3$ | $c_3$ | -739.87 | W/AU$^3$ |
| $a_4$ | 0 | | $b_4$ | 0 | | $c_4$ | 134.45 | W/AU$^4$ |

## 5 Time-optimal transfers

Performing a time-optimal search in a two-year departure window for different objects requires solving approximately $3.3 \times 10^5$ optimisation problems with a one-day time discretisation. The indirect solver LT2.0 (Low-Thrust Trajectory Optimiser 2.0) internally developed at Politecnico di Milano [12] has been adapted for this purpose. The dynamic model used is a standard two-body problem implementing the realistic thruster model in Section 4.2. Second-order effects such as third-body perturbation and solar radiation pressure will be implemented in following phases of the mission analysis.

### *5.1 Methodology*

The controlled two-body problem in Cartesian coordinates reads

$$\begin{cases} \dot{\boldsymbol{r}} = \boldsymbol{v} \\ \dot{\boldsymbol{v}} = -\dfrac{\mu}{r^3}\boldsymbol{r} + u\dfrac{T_{max}}{m}\boldsymbol{\alpha} \\ \dot{m} = -u\dfrac{T_{max}}{I_{sp}\, g_0} \end{cases} \tag{4}$$

where $\boldsymbol{r}$, $\boldsymbol{v}$, and $m$ are the spacecraft position vector, velocity vector, and mass, respectively, while $u \in [0, 1]$ is the throttle factor and $\boldsymbol{\alpha}$ is the thrust pointing unit vector; $g_0$ is the gravitational acceleration at sea level.
Consistently with the thruster model in Section 4.2, we have assumed that both the maximum thrust, $T_{max}$, and the specific impulse, $I_{sp}$, in Eq. (4) are assumed to vary with the engine input power $P_{in}$, which is in turn function of the Sun distance.
The initial time, $t_0$, is any epoch in the departure window 2023–2024. The initial condition is

$$\boldsymbol{r}(t_0) - \boldsymbol{r}_0 = 0, \quad \boldsymbol{v}(t_0) - \boldsymbol{v}_0 = 0, \quad m(t_0) - m_0 = 0 \tag{5}$$

In Eq. (5), $\boldsymbol{r}_0$ and $\boldsymbol{v}_0$ are the heliocentric position and velocity vectors as given by the Sun–Earth $L_2$ SPICE kernel. The kernel allows extracting position and velocity vectors as function of the departure epoch $t_0$; $m_0$ is instead the M-ARGO initial mass.
In the time-optimal problem, we want to rendezvous with a moving target. Therefore, the final time, $t_f$, and consequently the final mass, $m(t_f)$, are both free. The final, rendezvous conditions are therefore

$$\boldsymbol{r}(t_f) - \boldsymbol{r}_t(t_f) = 0, \quad \boldsymbol{v}(t_f) - \boldsymbol{v}_t(t_f) = 0 \tag{6}$$

where $\boldsymbol{r}_t(t)$ and $\boldsymbol{v}_t(t)$ are the position and velocity vectors of the target body, respectively. These two functions have been retrieved from the objects' SPICE kernels.
The objective function is

$$J = \int_{t_0}^{t_f} 1 \, \mathrm{d}t \tag{7}$$

and thus the Hamiltonian reads

$$H_t = \boldsymbol{\lambda}_r \cdot \boldsymbol{v} + \boldsymbol{\lambda}_v \cdot \left(-\frac{\mu}{r^3}\boldsymbol{r} + u\frac{T_{max}}{m}\boldsymbol{\alpha}\right) + -\lambda_m u \frac{T_{max}}{I_{sp}\, g_0} + 1 \tag{8}$$

The thrust pointing angle is such that $H_t$ is minimised at any time by virtue of the Pontryagin minimum principle (PMP)

$$\boldsymbol{\alpha}^*(t) = -\frac{\boldsymbol{\lambda}_v}{\lambda_v} \tag{9}$$

whereas it can be shown [13] that

$$u(t) = 1, \forall t \in [t_0,\, t_f] \tag{10}$$

This is to say that while the thrust magnitude is always set to the maximum available value, the thrust pointing angle is implicitly determined by the Lagrange multiplier $\boldsymbol{\lambda}_v$.
The problem is to find $\{\boldsymbol{\lambda}_0, t_f\}$ that allow integrating Eq. (4) and the costate dynamics (not reported for brevity sake), with the initial conditions in Eq. (5) and the implicit control policy in Eqs. (9)–(10) such that the solution zeroes the shooting function

$$\boldsymbol{\Gamma}_t(\boldsymbol{\lambda}_0, t_f) = \begin{pmatrix} \boldsymbol{r}(t_f) - \boldsymbol{r}_t(t_f) \\ \boldsymbol{v}(t_f) - \boldsymbol{v}_t(t_f) \\ \lambda_m(t_f) \\ H(t_f) - \boldsymbol{\lambda}_r(t_f) \cdot \boldsymbol{v}_t(t_f) - \boldsymbol{\lambda}_v(t_f) \cdot \boldsymbol{a}_t(t_f) \end{pmatrix} \tag{11}$$

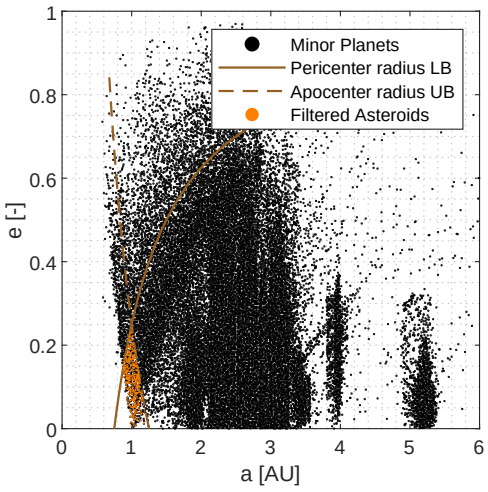


(a) $a$ vs $e$

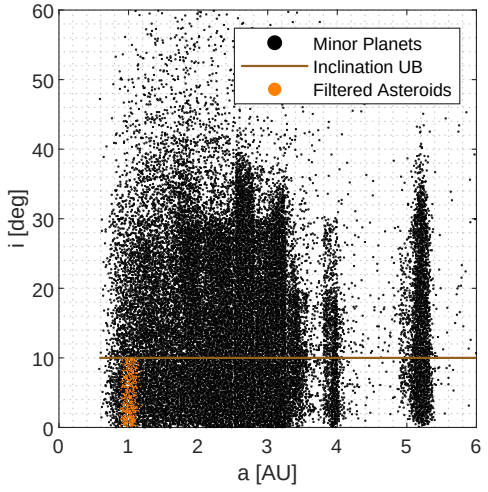


(b) $a$ vs $i$

Fig. 2: Minor planets semi-major axis ($a$), eccentricity ($e$), and inclination ($i$). The filtering bounds are the solid and dashed lines, while the filtered asteroids are highlighted in orange.

where $\boldsymbol{a}_t = \dot{\boldsymbol{v}}_t$
Optimising the transfer time produces solutions whose thrust is always set at the maximum available value. While these solutions are not feasible in practical applications, they yield the minimum theoretical transfer time,

$$\tau_{min} = \min_{t_0 \in [\underline{t}_0, \bar{t}_0]} \tau(t_0) \tag{12}$$

where $\tau(t_0) := t_f(t_0) - t_0$ and $[\underline{t}_0, \bar{t}_0]$ is the two-year departure window.

### 5.2 *Search space pruning*

For each of the asteroids processed, $\tau_{min}$ is retrieved, as well as its corresponding propellant mass $m_P(\tau_{min})$. The two quantities are reported in Figure 5 in the form of cumulative distribution functions. These information have been used to further reduce the set of asteroids that can be reached by M-ARGO using the "up to 3 years" and "up to 2.8 kg" requirements. Considering that the *real* transfer time has to be greater than the one resulting from time-optimal computations, the following criteria have been used:

1) Minimum theoretical transfer time lower than of 900 days: $\tau_{min} \leq 900$ days. There are 299 asteroids out of the processed satisfying this condition, see Figure 5a.

2) Minimum propellant mass lower than of 4 kg; $m_p(\tau_{min}) \leq 4$ kg. There are 181 asteroids out of the processed whose minimum propellant mass is below this threshold[1], see Figure 5b.

Then, these two conditions are imposed together. The graphical representation in Figure 6 shows that the propellant mass condition is the more stringent one. As a result of this pruning process, 172 asteroids are ranked in terms of transfer time. This list of asteroids is the input of the fuel-optimal step as per the approach in Figure 1. Inspection of Figure 6 reveals that the points therein are the solution of the following differential equation

$$\dot{m} = -\frac{T_{max}(P_{in}(t))}{g_0\, I_{sp}(P_{in}(t))} \tag{13}$$

because $u(t) = 1\ \forall t \in [t_0\, t_f]$. Differently from the standard cases in which $T_{max}$ and $I_{sp}$ are both constant, Eq. 13 cannot be solved in closed form because $P_{in} = P_{in}(r(t))$. However, for inbound transfers, we ave that $P_{in}(t) = P_{max}$, and thus Eq. (13) becomes

$$\tau_{min} = \frac{g_0\, I_{sp}(P_{max})}{T_{max}(P_{max})} m_p \tag{14}$$

Eq. (14) is the equation of a straight line whose slope is $g_0\, I_{sp}(P_{max})/T_{max}(P_{max})$. This line bounds the points in Figure 6 and can be used to infer the following:

- For a given propellant mass, inbound targets tend to take shorter than outbound ones;
- For a given transfer time, outbound targets need less propellant than inbound ones.

[1] In a previous iteration this threshold was set to 3.5 kg, yielding 125 asteroid that passed the test. Since this was perceived a bit restricting, the cutoff value has been moved to 4 kg, resulting in 181 potential targets.

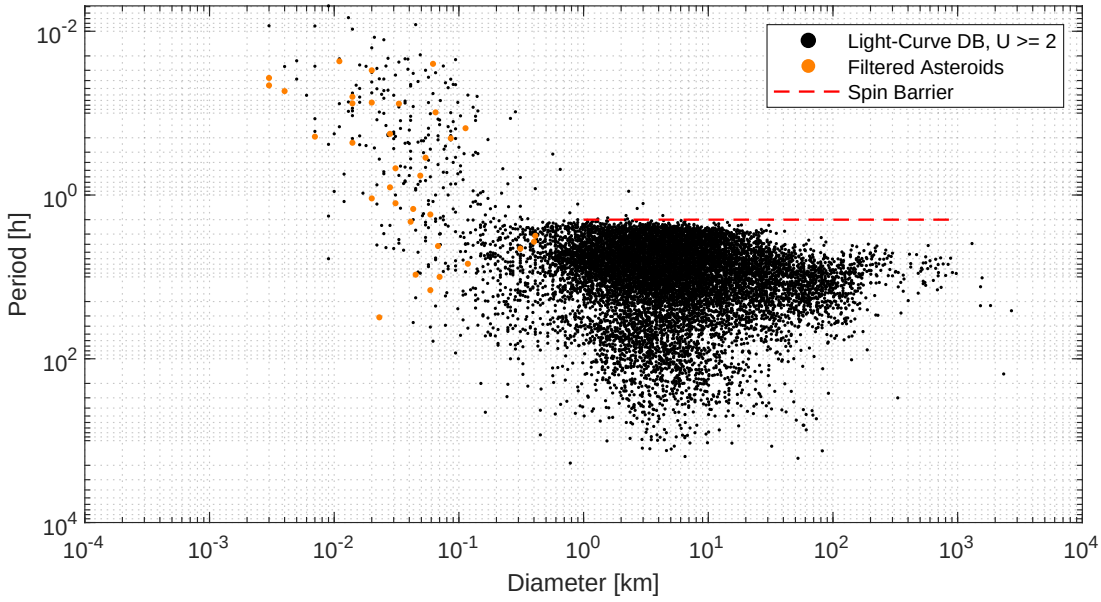


Fig. 3: Rotational period against diameter for minor planets. Filtered asteroids in orange. Data retrieved from the asteroid Light-Curve database.

## 6 Fuel-optimal transfers

The 172 potential targets that passed the time-optimal pruning have been processed under the perspective of a fuel-optimal step. It is worth highlighting that the fuel-optimal process widens the variable space as both the departure epoch $t_0$ and the time of flight $tof$ are let to vary. That is, while time-optimal problems have a one-dimensional search space ($t_0$), the fuel-optimal problems have a two-dimensional search space ($[t_0, tof]$). A two-dimensional grid is therefore used for the porkchop plots[1].

### *6.1 Methodology*

The minimum-fuel optimisation has been performed by using the same model as in the minimum-time optimisation, Eq. (4). For each departure day $t_0$, the time of flight $tof$ is bottomed by the corresponding minimum transfer time $\tau(t_0)$ and capped by $\overline{\tau}$, the 3-years upper bound condition. This variable range has been discretised using a nonuniform grid, to ease efficiency. The boundary conditions are those in Eqs. (5) and (6).
The objective function is the used propellant mass

$$J = \int_{t_0}^{t_f} u \frac{T_{max}}{I_{sp}\, g_0}\, \mathrm{d}t \tag{15}$$

[1]In practice, the search space of fuel-optimal transfers is three-dimensional because there is an homotopy parameter that is used to map energy-optimal problems into fuel-optimal problems [13]

With a two-dimensional search space, the propellant mass varies for any combination of departure $t_0$ and $tof$. The Hamiltonian of the problem is

$$H = \boldsymbol{\lambda}_r \cdot \boldsymbol{v} + \boldsymbol{\lambda}_v \cdot \left(-\frac{\mu}{r^3}\boldsymbol{r} + u\frac{T_{max}}{m}\boldsymbol{\alpha}\right) + \lambda_m \left(-u\frac{T_{max}}{I_{sp}\, g_0}\right) + u\frac{T_{max}}{I_{sp}\, g_0} \tag{16}$$

whose minimisation (by virtue of the PMP) yields once again the thrust pointing law as in Eq. (9) and the following throttling law

$$u^* = \begin{cases} 0 & \text{if } S > 0 \text{ or } P_{in} < P_{min} \\ 1 & \text{if } S < 0 \text{ and } P_{in} \geq P_{min} \\ \in [0,1] & \text{if } S = 0 \text{ and } P_{in} \geq P_{min} \end{cases} \tag{17}$$

where the throttle switching function $S$ is

$$S = \frac{T_{max}}{I_{sp}\, g_0}\left(1 - \lambda_m - \frac{I_{sp}\, g_0}{m}\lambda_v\right) \tag{18}$$

The problem is to find $\boldsymbol{\lambda}_0$ that allows integrating Eq. (4) and the costate equations (not shown for brevity), with the initial conditions (5) and the implicit control structure in Eq. (9) and (17) such that the solution zeroes the shooting function

$$\boldsymbol{\Gamma}(\boldsymbol{\lambda}_0) = \begin{pmatrix} \boldsymbol{r}(t_f) - \boldsymbol{r}_f \\ \boldsymbol{v}(t_f) - \boldsymbol{v}_f \\ \lambda_m(t_f) \end{pmatrix} \tag{19}$$

The outcome of the minimum-fuel optimisation is shown for four sample targets in Figure 7. The colored area

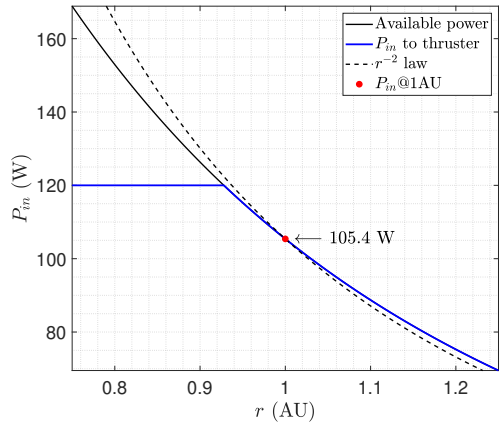


(a) $P_{in}$ versus $r$

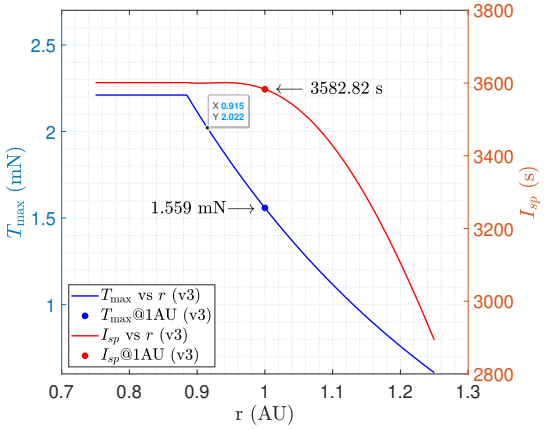


(b) $T_{max}$ and $I_{sp}$ versus $r$

Fig. 4: Graphical representation of the thruster model.

represents the search space: departure day ($t_0$) on the $x$-axis, transfer time ($tof$) on the $y$-axis; the color code indicates the propellant mass used for each combination of this two variables, $m_p(t_0, tof)$ (see the colored bars on the right). The red thick lines are the minimum-time profiles. The dashed region below the red line is therefore unfeasible: for a given departure day, M-ARGO cannot take shorter then the corresponding point on the red line.

Worth to extract is the global minimum of the propellant mass function, that is

$$m_{p,min} = \min_{\substack{t_0 \in [\underline{t}_0, \overline{t}_0] \\ tof \in [\tau(t_0), \overline{\tau}]}} m_p(t_0, tof) \tag{20}$$

Graphically, $m_{p,min}$ is the blue-most point in the pork-chop plots.

### 6.2 *Search space pruning*

For the 172 asteroid processed, $m_{p,min}$ is retrieved, as well as the corresponding value of $t_0$ and $tof$. The global minimum propellant mass $m_{p,min}$ is shown in the form of a cumulative distribution function in Figure 8. This information has been used to further reduce the search space by enforcing the "up to 2.8 kg" requirement. It can be seen that **148 asteroids result feasible** when enforcing this requirement.

Figure 9 shows instead the global minimum propellant mass $m_{p,min}$ against the associated $tof$. Comparing this figure with Figure 6 one can notice that the minimum-fuel optimisation trades propellant mass for transfer time: the majority of the solutions have their $m_{p,min}$ just below $\overline{\tau}$, the 3-year maximum transfer duration.

## 7 Targets selection

With reference to the methodology developed for the NEO target screening, out of more than 900,000 minor bodies in the MPC database, 456 objects passed the pre-filtering, which was based on simple geometrical criteria. For these 456 objects, a minimum-time optimisation was carried out, and a subset made of 172 targets passed the pruning process when enforcing both a transfer time and a propellant mass thresholds (Section 5). These asteroids were then processed under the perspective of a minimum-fuel optimisation, and a subset of them made of 148 *reachable targets* was found (Section 6).

The whole process undertaken as well as the intermediate results are summarised in Table 3 (steps #1–#4). The focus is now on extracting a shortlist of 5 baseline asteroids out of the 148 reachable targets. This has been done through: 1) Statistical analysis of the reachable targets and their transfers; 2) Detailed analysis of pork chop plots; 3) Close-up analysis of the downselected targets. The analysis in 1)–2) produces the list of downselected asteroids (step #5 in Table 3), while the outcome of 3) is the list of the 5 targets selected (step #6 in Table 3).

## 8 Statistics of the reachable targets and transfers

Figures 10 report the statistical distribution of the reachable targets in terms of inclination $i$ (Figure 10a), absolute magnitude $H$ (Figure 10b), aphelion (Figure 10c) and perihelion (Figure 10d). As for the inclination, asteroids having $i$ of up to 6 deg are reachable, which validates our choice of considering targets with $i \geq 5$ deg in the pre-filtering. As for the magnitude range, the minimum value of $H$ is 22.5, which means the the reachable

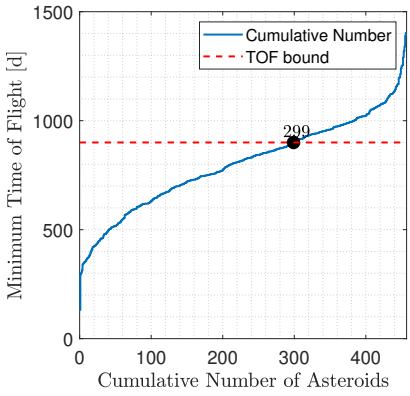


(a) Cumulative Asteroids number vs $\tau_{min}$

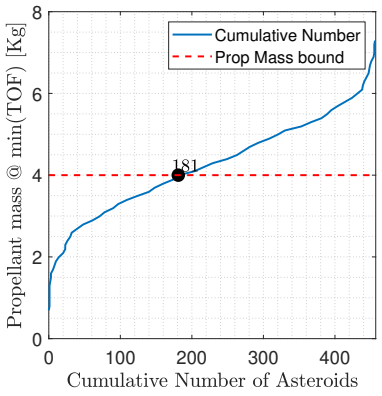


(b) Cumulative Asteroids number vs $m_p(\tau_{min})$

Fig. 5: Cumulative number of asteroids for increasing $\tau_{min}$ and associated $m_p(\tau_{min})$. The filtering bounds are the dashed lines, while the number indicates the asteroids below the threshold.

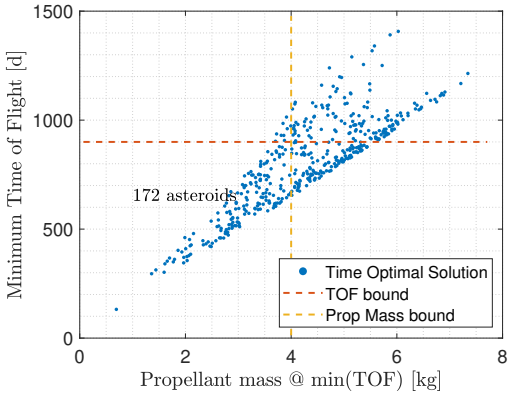


Fig. 6: Time of Flight for the time-optimal solutions against the associated propellant mass. The filtering bounds are the dashed lines, while the number indicates the asteroids below both thresholds.

Tab. 3: NEO target screening process and results.

| **Step** | **Target screening step** | **No. of objects** |
|---|---|---|
| #1 | Asteroids in the Minor Planet Center database | 900,000+ |
| #2 | Potential targets after orbital parameters pre-filtering | 456 |
| #3 | Possible targets after minimum-time optimisation and pruning | 172 |
| #4 | Reachable targets after minimum-fuel optimisation and pruning | 148 |
| #5 | Downselected targets after statistical, pork chop analysis | 41 |
| #6 | Shortlisted targets after close-up analysis | 5 |

objects are quite faint – and therefore small. The aphelion ranges between 1 and 1.24 AU (Figure 10c), while the perihelion ranges between 0.75 and 1.175 AU (Figure 10d).

In Figure 11, a simple statistical distribution of the transfers to the reachable asteroids is shown in terms of propellant mass and transfer time. As for the propellant mass, it can be seen that approximately 10 targets can be reached using less than 1 kg propellant. The majority of the transfers requires approximately 1.4–2.2 kg of propellant, and by definition all of them are below the 2.8 kg cut off value (see Figure 11a). The distribution of $tof$ is instead more unbalanced. From Figure 11b it can be seen that the vast majority of fuel-optimal solutions tend to have the time of flight associated to the global optimum toward the upper bound of 1100 days. This is

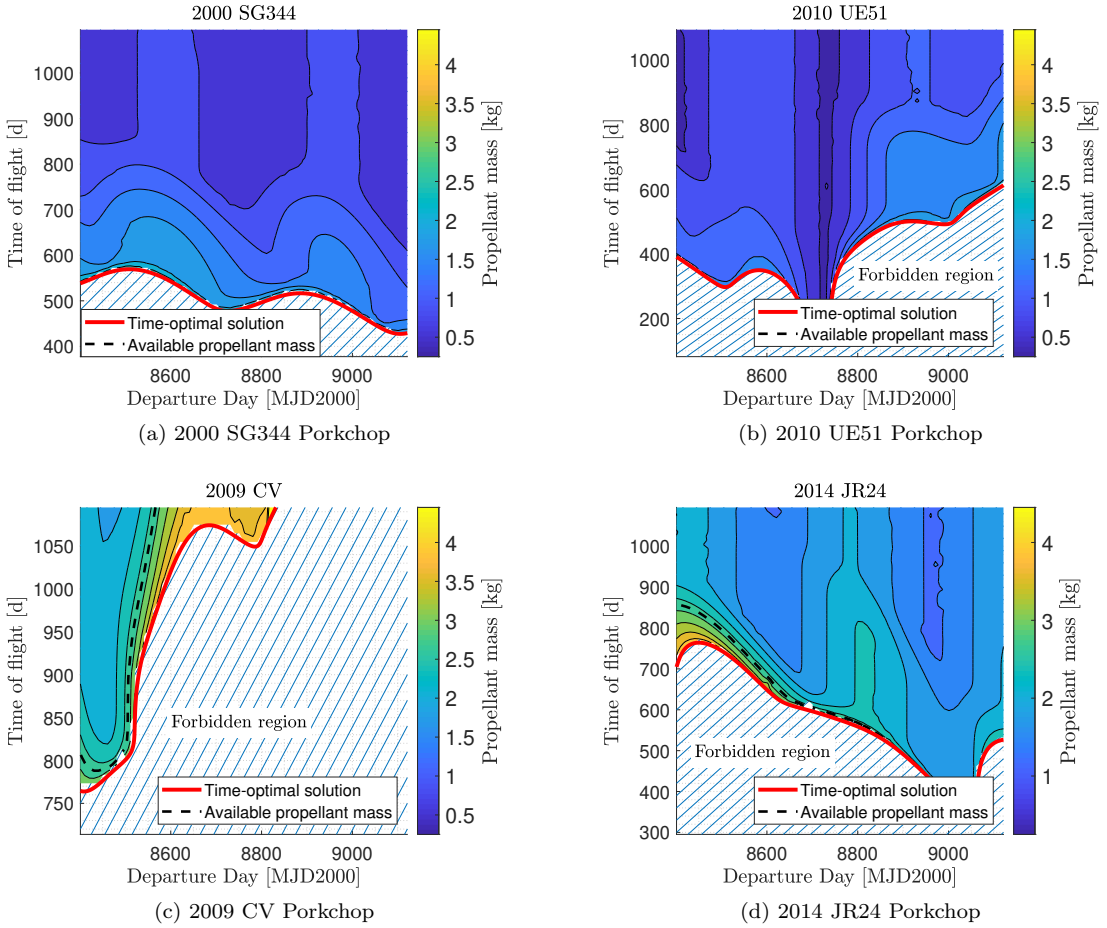


(a) 2000 SG344 Porkchop

(b) 2010 UE51 Porkchop

(c) 2009 CV Porkchop

(d) 2014 JR24 Porkchop

Fig. 7: Porkchop-like plots for some sample asteroids. The available propellant mass ($m_p = 2.8$ kg) is indicated with a black dashed line, while the red thick line shows the time-optimal solution. The color code is the propellant mass used, see the bars on the right.

not surprisingly, as it was expected that in minimum-fuel optimisation the propellant mass is traded for time of flight. Therefore, a trade off between these two variables is needed when selecting the baseline (and backup) solutions for the shortlisted targets.

## 9 Analysis of pork chop plots

A close look at the 148 *feasible* pork chop plots suggests that the search space can be restricted by excluding those targets for which

A. The transfer requires long time of flights;

B. The transfer requires high propellant mass;

C. The departure opportunities do not span the full departure window.

By enforcing criteria A, B, and C above, many targets can be excluded from the subsequent analysis. In particular, 40 asteroids are found to have a long transfer time (condition A), 31 asteroids have a relatively high propellant mass (condition B), and 36 asteroids do not span the full departure window (condition C). Thus, a total of 107 asteroids are excluded from the solution space.

## 10 List of downselected targets

After pruning out the search space by enforcing criteria A, B, and C in Section 9, the 41 targets listed in Table 4 are found. These targets are all reachable, and in principle all of them can be considered in the subsequent shortlist.

Figures 13 and 12 report the statistical distribution of the downselected targets (in brown) over the same information for the reachable targets (in blue, reported in Figures 10 and 11). From the inclination distribution in Figure 13a it can be inferred that the downselected targets lie in the less inclined range of orbits, while the magnitude, aphelion, and perihelion distributions do not

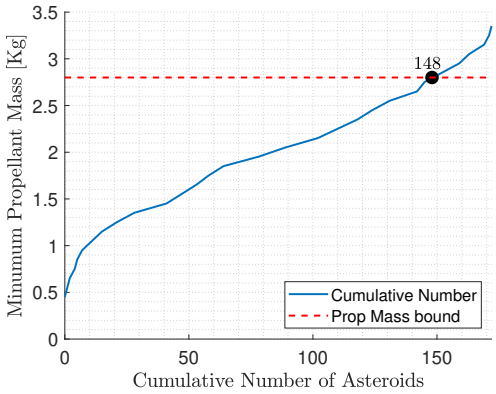


Fig. 8: Cumulative number of asteroids for increasing global minimum propellant mass. The available propellant mass ($m_p = 2.8$ kg) is indicated by the dashed line, while the number shows the amount of asteroids below the threshold.

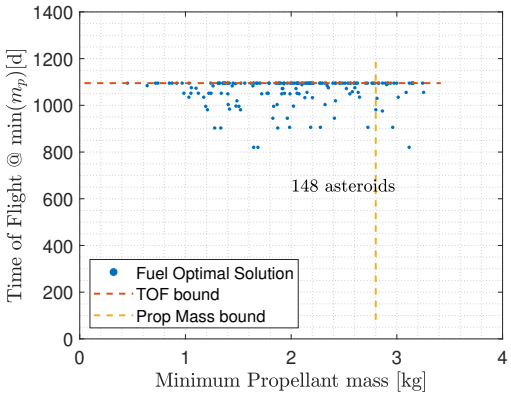


Fig. 9: Propellant mass for the fuel-optimal solutions against the associated time of flight. The filtering bounds are the dashed lines, while the number indicates the asteroids below the threshold.

Tab. 4: List of downselected targets.

| **Downselected targets (41)** |
|---|
| 2012 UV136, 2000 SG344, 2001 QJ142, 2008 CM74, 2008 DL4, 2008 HU4, 2008 JL24, 2008 ST, 2009 BD, 2010 JR34, 2010 UE51, 2011 BQ50, 2011 MD, 2011 WU2, 2012 BB14, 2012 EP10, 2012 TF79, 2014 JR24, 2014 LJ, 2014 YD, 2014 YN, 2015 BM510, 2015 KK57, 2015 VU64, 2015 VO142, 2015 XZ378, 2016 BQ, 2016 CF137, 2016 DF, 2016 FU12, 2016 TB18, 2016 TB57, 2016 WQ3, 2017 DV35, 2017 RL2, 2017 YW3, 2018 DC4, 2018 GE, 2019 AP8, 2019 DJ1, 2019 GF1 |

show any particular trend (Figures 13b–13d).
The propellant mass and the transfer time associated to the downselected targets (in brown) are shown in Figure 12 against the same data for the reachable targets (in blue, reported in Figure 11). From the propellant distribution in Figure 12a, we can see that searching for "the most blue" regions in the porkchop plots meant selecting the targets that take less propellant. Out of these, 8 targets take less than 1 kg of propellant mass, while all of them take less than 2 kg. From the transfer time distribution in Figure 12b, we can see that the *tof* associated to the minimum-fuel solutions covers all the range.

## 11 Shortlist of targets

Once the list of the 41 downselected targets has been defined, a deliberate choice has to be made. This choice considers the available of information on the asteroid light-curve, spin-rate, and observability in the future to further downselect the targets.

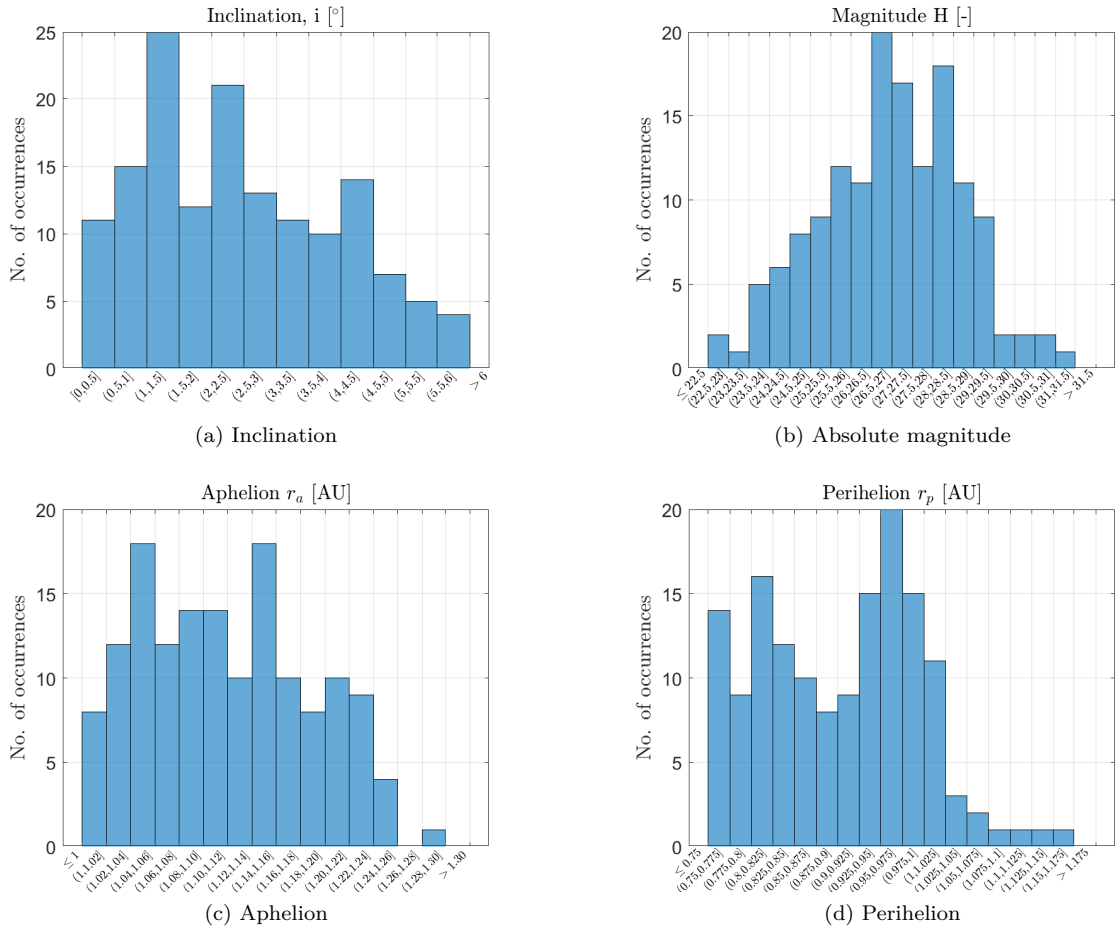


(a) Inclination (b) Absolute magnitude

(c) Aphelion (d) Perihelion

Fig. 10: Statistics of the reachable targets.

As a result of this exercise, the three top picks for the initial selection are:

1. **2014 YD**: Known high spin rate close to spin barrier and favourable mission opportunity;
2. **2010 UE51**: #1 on time-optimal and fuel-optimal solution list;
3. **2011 MD**: Present in light curve database; Favourable mission opportunity.

Moreover, two more asteroids have been liberally chosen based on their solar distances, Earth distances, size/magnitude, departure opportunity, etc.; the two additional targets are:

4. **2000 SG344**: Chance for observation, higher inclination, good OCC;
5. **2012 UV136**: Known spin rate, largest target size/brightest.

The orbital parameters of these 5 targets are reported in Table 5. The porkchops of these 5 shortlisted targets are shown in Figure 14.

## 12 Conclusions

This paper has reported the NEO targets screening for the M-ARGO mission. In order to select the mission targets, a series of asteroids filtering activities have been performed to identify a subset of asteroids that are reachable by the M-ARGO CubeSat. The downselection procedure started by consulting the Minor Planet Center database and ended up with a set of 5 shortlisted targets. First, bounds on orbital elements have reduced the list of asteroids to 456 objects. Out of these, 172 objects require less than 3 years for the time-optimal solution, and 148 require less than 2.8 kg for the fuel-optimal solution. Then, out of 148 objects completely reachable by the M-ARGO CubeSat, 5 asteroids have been selected as potential targets for the mission. This filtering step was required to assess the mission feasibility in terms of availability of targets given the M-ARGO 12U CubeSat spacecraft and mission characteristics.

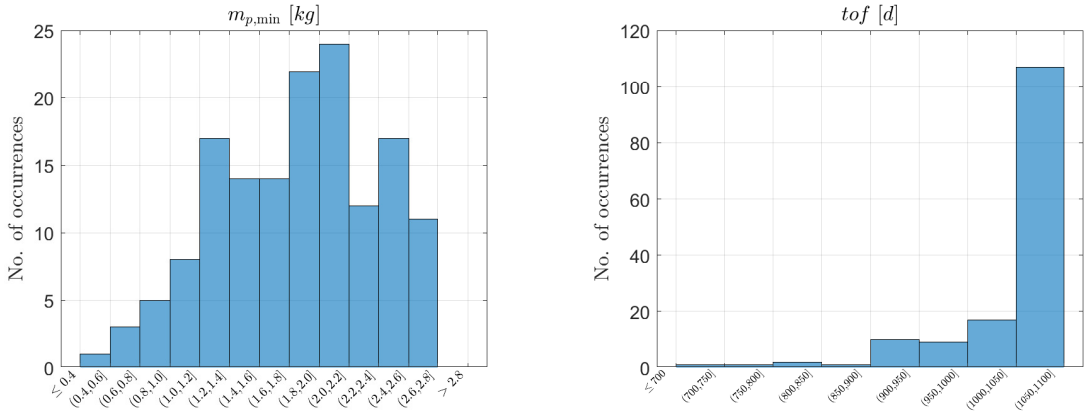


(a) Propellant mass (b) Time of flight

Fig. 11: Statistics of the transfers to the reachable targets.

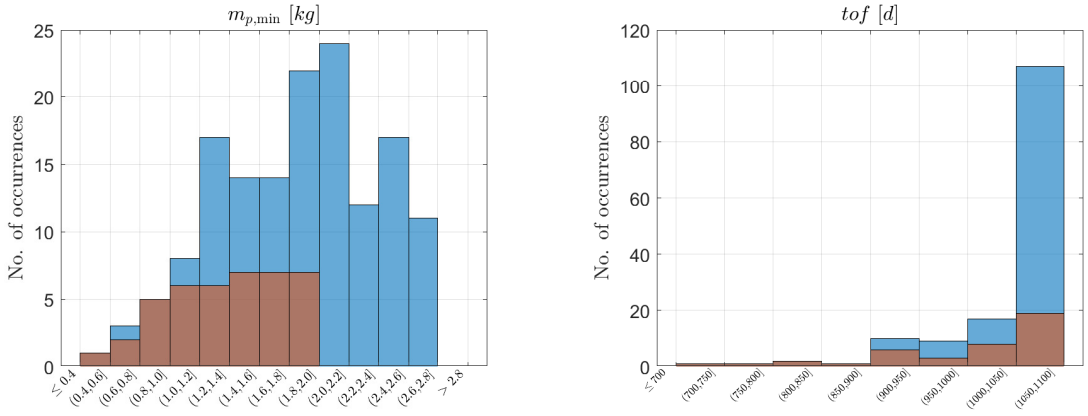


(a) Propellant mass (b) Time of flight

Fig. 12: Statistics of transfers to the downselected targets (brown).

Tab. 5: Orbital elements for the selected 5 asteroids (ecliptic J2000).

| Name | a [AU] | e [-] | i [deg] | $\omega$ [deg] | $\Omega$ [deg] |
|---|---|---|---|---|---|
| 2000 SG344 | 0.9775 | 0.0669 | 0.1121 | 275.3026 | 191.9599 |
| 2010 UE51 | 1.0552 | 0.0597 | 0.6239 | 47.2479 | 32.2993 |
| 2011 MD | 1.0562 | 0.0371 | 2.4455 | 5.9818 | 271.5986 |
| 2012 UV136 | 1.0073 | 0.1392 | 2.2134 | 288.6071 | 209.9001 |
| 2014 YD | 1.0721 | 0.0866 | 1.7357 | 34.1161 | 117.6401 |

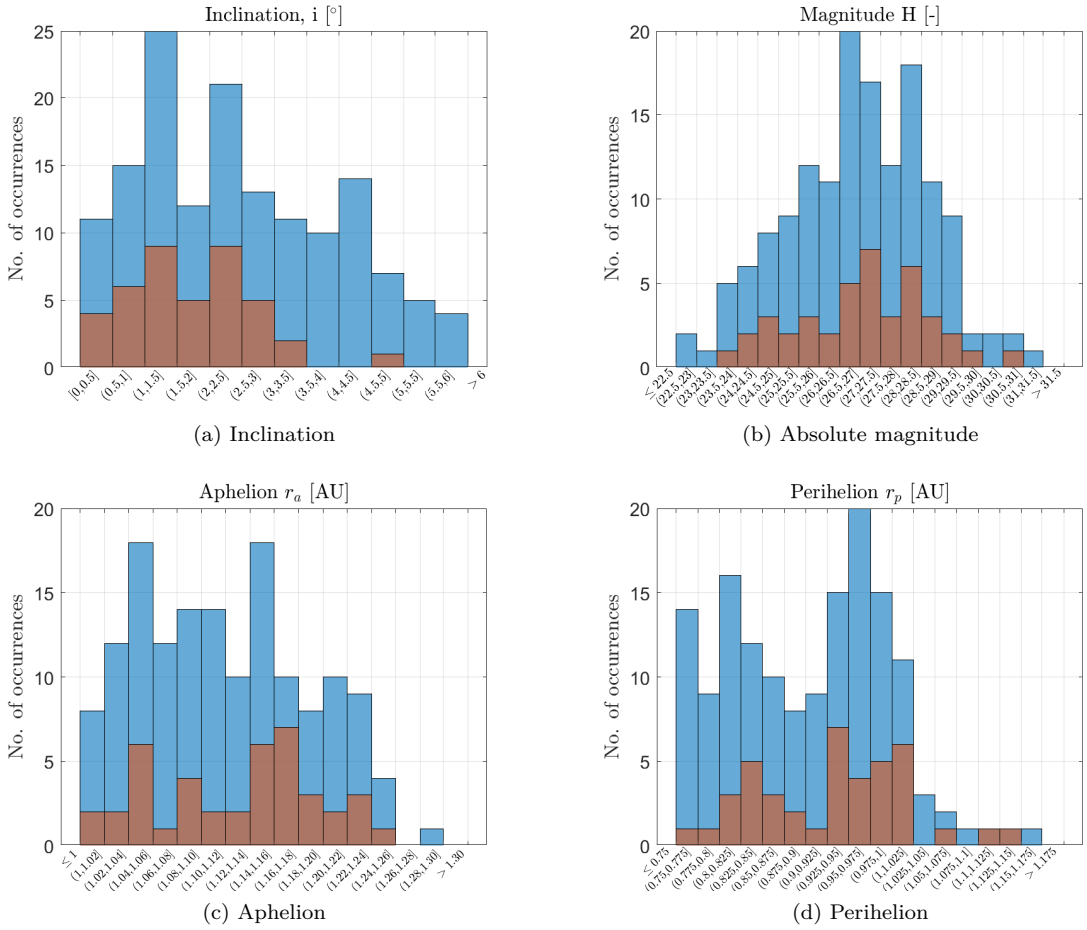


(a) Inclination (b) Absolute magnitude

(c) Aphelion (d) Perihelion

Fig. 13: Statistics of the downselected targets (brown).

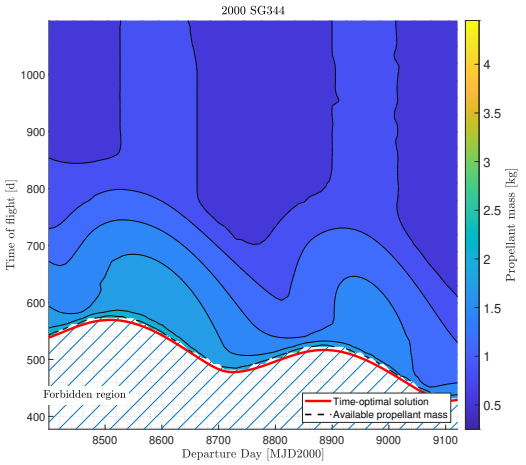


(a) 2000 SG344 pork chop plot

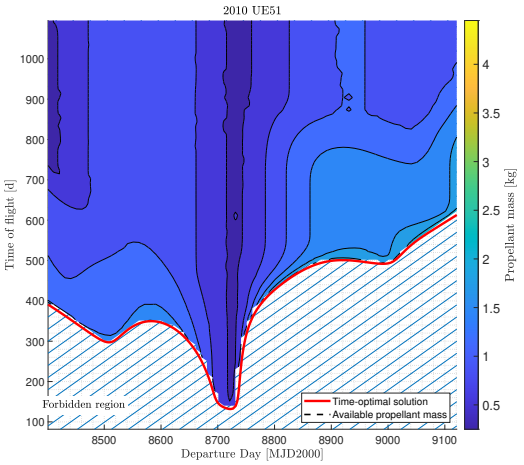


(b) 2010 UE51 pork chop plot

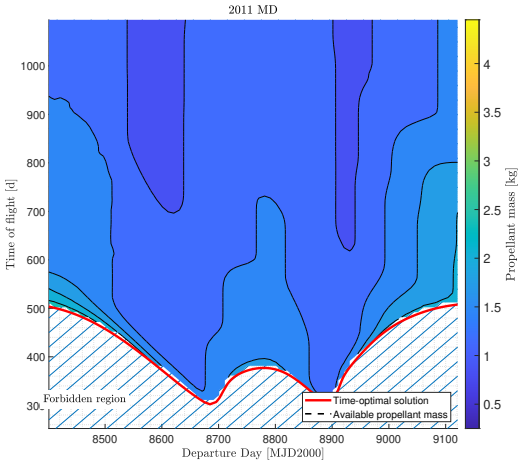


(c) 2011 MD pork chop plot

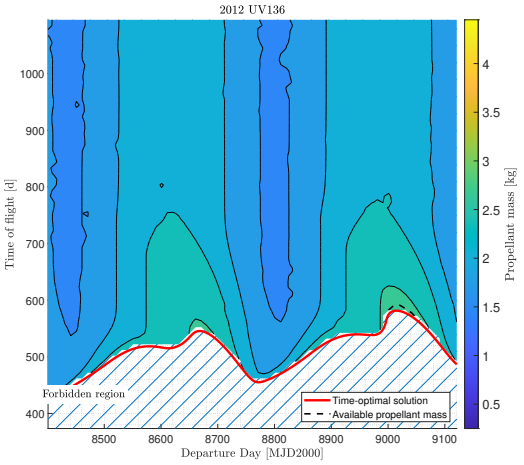


(d) 2012 UV136 pork chop plot

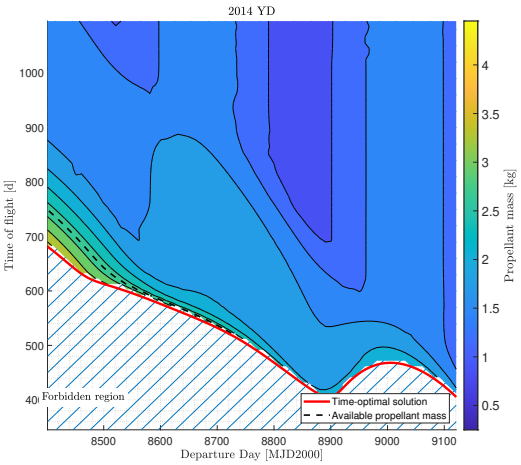


(e) 2014 YD pork chop plot

Fig. 14: Pork chop plots of short listed targets.

## Acknowledgments

This work has been conducted under ESA Contract No. 4000127373/19/NL/AF. The authors would like to thank Franco Perez Lissi for his helpful contributions.

## Bibliography

[1] R. Walker, D. Binns, C. Bramanti, M. Casasco, P. Concari, D. Izzo, D. Feili, P. Fernandez, J. Fernandez, P. Hager, et al. Deep-space cubesats: thinking inside the box. *Astronomy & Geophysics*, 59(5):5–24, 2018. DOI: 10.1093/astrogeo/aty237.

[2] R. Walker, D. Koschny, C. Bramanti, I. Carnelli, et al. Miniaturised asteroid remote geophysical observer (M-ARGO): a stand-alone deep space cubesat system for low-cost science and exploration missions. In *iCubeSat Workshop*, pages 1–20, Cambridge, 2017.

[3] V. Franzese, P. Di Lizia, and F. Topputo. Autonomous optical navigation for the lunar meteoroid impacts observer. *Journal of Guidance, Control, and Dynamics*, 42(7):1579–1586, 2019. DOI: 10.2514/1.G003999.

[4] F. Topputo, M. Massari, J. Biggs, P. Di Lizia, D. Dei Tos, K. Mani, S. Ceccherini, V. Franzese, A. Cervone, P. Sundaramoorthy, et al. LUMIO: a cubesat at earth-moon l2. In *4S Symposium*, pages 1–15, Sorrento, 2018.

[5] S. Speretta, A. Cervone, P. Sundaramoorthy, R. Noomen, S. Mestry, A. Cipriano, F. Topputo, J. Biggs, P. Di Lizia, M. Massari, K. Mani, D. Dei Tos, S. Ceccherini, V. Franzese, A. Ivanov, D. Labate, L. Tommasi, A. Jochemsen, J. Gailis, R. Furfaro, V. Reddy, J. Vennekens, and R. Walker. *LUMIO: An Autonomous CubeSat for Lunar Exploration*, chapter 6, pages 103–134. Springer International Publishing, 2019. DOI: 10.1007/978-3-030-11536-4_6.

[6] A. Cipriano, D. Dei Tos, and F. Topputo. Orbit design for LUMIO: The lunar meteoroid impacts observer. *Frontiers in Astronomy and Space Sciences*, 5:29, 2018. DOI: 10.3389/fspas.2018.00029.

[7] P. Michel, M. Küppers, and I. Carnelli. The Hera mission: European component of the ESA–NASA AIDA mission to a binary asteroid. In *42nd COSPAR Scientific Assembly*, volume 42 of *COSPAR Meeting*, pages 1–42, July Pasadena, California, 2018.

[8] A. Klesh and J. Krajewski. MarCO: Cubesats to mars in 2016. In *29th Annual AIAA/USU Conference on Small Satellites*, pages 1–7, Logan, UT, 2015.

[9] A. Mereta and D. Izzo. Target selection for a small low-thrust mission to near-earth asteroids. *Astrodynamics*, 2(3):249–263, 2018. DOI: 10.1007/s42064-018-0024-y.

[10] R. Walker, D. Binns, C. Bramanti, M. Casasco, P. Concari, D. Izzo, D. Feili, P. Fernandez, J. Fernandez, P. Hager, et al. M-ARGO, assessment of standalone interplanetary cubesat mission. CDF Study Report, 2017.

[11] H. Goldberg. M-ARGO solar cell and electric propulsion model. Technical Note, July 2019.

[12] F. Topputo, D. Dei Tos, K. Mani, S. Ceccherini, C. Giordano, V. Franzese, and Y. Wang. Trajectory design in high-fidelity models. In *7th International Conference on Astrodynamics Tools and Techniques (ICATT), 6-9 November 2018, Oberpfaffenhofen, Germany*, 2018.

[13] C. Zhang, F. Topputo, F. Bernelli-Zazzera, and Y. Zhao. Low-thrust minimum-fuel optimization in the circular restricted three-body problem. *Journal of Guidance, Control, and Dynamics*, 38(8):1501–1510, 2015. DOI: 10.2514/1.G001080.